Available online at www.sciencedirect.com
ScienceDirect
Journal of Hazardous Materials 153 (2008) 701–708
Journal of Hazardous Materials
www.elsevier.com/locate/jhazmat

Kinetics and equilibrium studies of malachite green adsorption on rice straw-derived char

B.H. Hameed [a,*], M.I. El-Khaiary [b]

[a] School of Chemical Engineering, Engineering Campus, Universiti Sains Malaysia, 14300 Nibong Tebal, Penang, Malaysia
[b] Chemical Engineering Department, Faculty of Engineering, Alexandria University, El-Hadara, Alexandria 21544, Egypt

Received 16 July 2007; received in revised form 31 August 2007; accepted 3 September 2007
Available online 8 September 2007

Abstract

In this work, the potential feasibility of rice straw-derived char (RSC) for removal of C.I. Basic Green 4 (malachite green (MG)), a cationic dye from aqueous solution was investigated. The isotherm parameters were estimated by non-linear regression analysis. The equilibrium process was described well by the Langmuir isotherm model. The maximum RSC sorption capacity was found to be 148.74 mg/L at 30 °C. The kinetics of MG sorption on RSC followed the Lagergren's pseudo-first-order model and the overall rate of dye uptake was found to be controlled by external mass transfer at the beginning of adsorption, while intraparticle diffusion controlled the overall rate of adsorption at a later stage. The results indicated that RSC was an attractive adsorbent for removing basic dye from aqueous solutions.

Keywords: Rice straw; Char; Malachite green; Adsorption isotherm; Kinetics

1. Introduction

Malachite green is widely used in aquaculture as a parasiticide and in food, health, textile and other industries for one or the other purposes. It controls fungal attacks, protozoan infections and some other diseases caused by helminths on a wide variety of fish and other aquatic organisms. However, the dye has generated much concern regarding its use, due to its reported toxic effects [1]. Though the use of this dye has been banned in several countries and not approved by US Food and Drug Administration [2], it is still being used in many parts of the world due to its low-cost, ready availability and efficacy [3] and to lack of a proper alternative. Its use in the aquaculture practice in many countries, including Malaysia has not been regulated [4]. Many adverse effects from the consumption of the dye due to its carcinogenic, genotoxic, mutagenic and teratogenic properties in animal studies have been reported [5].

Various attempts have been made for its removal from the wastewater. These include photo-degradation [6,7], photocatalytic degradation [8–10] and adsorption.

Adsorption process has become one of the most effective and comparable low-cost method for the removal of dyes from aqueous solutions. Adsorption of malachite green (MG) on activated carbon has been reported [4,11]. Also a number of non-conventional sorbents has been studied in the literature for their capacity to remove malachite green from aqueous solutions, such as de-oiled soya [12], agro-industry waste, *Prosopis cineraria* [13], bottom ash [14], hen feathers [15], iron humate [16] and modified rice straw [17].

In this work, we attempt to utilize rice straw, which are discarded as waste material from the food industry, to prepare char for the removal of malachite green from aqueous solutions. Rice straw (*Oryza sativa*) is one of the abundant lignocellulosic waste materials in the world. Ninety percent of the world's production is in developing countries of East and Southeast Asia where the straw is a main feed for ruminants [18]. Rice straw is a lignocellulosic agricultural by-product containing cellulose (37.4%), hemi-cellulose (44.9%), lignin (4.9%) and silicon ash (13.1%) [19]. The estimation on annual production of rice by FAO points to about 600 million tonnes per year in 2004. On the other hand, every kilogram of grain harvested is accompanied by production of 1–1.5 kg of the straw [20,21]. Thus rice straw causes the most environmental problem since it exists with enormous quantities and is not easy to handle or transport. Therefore, direct open

* Corresponding author. Fax: +604 594 1013.
E-mail address: chbassim@eng.usm.my (B.H. Hameed).

0304-3894/$ – see front matter © 2007 Elsevier B.V. All rights reserved.
doi:10.1016/j.jhazmat.2007.09.019

burning in fields is a common option for disposal. This option causes serious air pollution, hence new economical methods for rice straw disposal and utilization must be developed. In this paper, we attempt to reduce the adverse impact on the environment and to use this renewable biomass to produce char for removal of basic dye from aqueous solutions. This would add value to this agricultural commodity and provide a potentially cheap alternative to existing commercial activated carbons.

The objective of this work is to investigate the potential feasibility of using of rice straw (agricultural residue) biomass-derived char for removing malachite green from aqueous solutions.

2. Materials and methods

2.1. Adsorbate

The dye, malachite green oxalate, C.I. Basic Green 4, C.I. Classification Number 42,000, chemical formula = $C_{52}H_{54}N_4O_{12}$, MW = 927.00, λ_{max} = 618 nm (measured value) was supplied by Sigma–Aldrich (M) Sdn Bhd, Malaysia and used as received. Stock solutions were prepared by dissolving accurately weighed samples of dye in distilled water to give a concentration of 1000 mg/L and diluting when necessary.

2.2. Char preparation

The rice straws used for preparation of char was procured locally, washed, dried and chopped to ca. 2–3 cm in length. Char preparation was carried out in a stainless steel vertical tubular reactor placed in a tube furnace at a heating rate of 20–700 °C with 2 h soaking time. A constant nitrogen (99.995%) flow of 150 mL/min was used. The char product was then cooled to room temperature and washed with hot deionized water and hydrochloric acid of 0.1 M until the pH of the washing solution reached 6–7. Then the char was oven dried at 105 °C, ground, sieved to obtain a particle size of 32–42 mesh and stored in plastic bottle for further use.

2.3. Effect of solution pH

In this study, the effect of solution pH was studied by agitating 0.30 g of rice straw-derived char (RSC) and 200 mL of dye solution of dye concentration 100 mg/L using water-bath shaker at 30 °C. The experiment was conducted at different pH from 2 to 7. Agitation was provided for 2 h contact time which is sufficient to reach equilibrium with a constant agitation speed of 130 rpm. The solution pH was adjusted using a pH meter (Ecoscan, EUTECH Instruments, Singapore) by adding drop wise 0.1N NaOH or 0.1N HCl solution before experiments started.

2.4. Kinetic studies

Kinetic experiments were identical to those of equilibrium tests. The aqueous samples were taken at preset time intervals and the concentrations of MG were similarly measured. All the kinetic experiments were carried out at pH 5. The amount of sorption at time t, q_t (mg/g), was calculated by:

$$q_t = \frac{(C_0 - C_t)V}{W} \quad (1)$$

where C_t (mg/L) is the liquid-phase concentrations of dye at any time.

2.5. Equilibrium studies

Batch adsorption isotherms were carried out by adding a fixed amount of sorbent (0.30 g) into 250-ml Erlenmeyer flasks containing 200 ml of different initial concentrations (25–300 mg/L) of dye solution at pH 5. The flasks were agitated in an isothermal water-bath shaker at 130 rpm and 30 °C for 2 h until equilibrium was reached. Aqueous samples were taken from the solutions and the concentrations were analyzed. At time $t = 0$ and at equilibrium, the dye concentrations were measured by a double beam UV/Vis spectrophotometer (Shimadzu, Model UV 1601, Japan) at 618 nm. The amount of equilibrium adsorption, q_e (mg/g), was calculated by:

$$q_e = \frac{(C_0 - C_e)V}{W} \quad (2)$$

where C_0 and C_e (mg/L) are the liquid-phase concentrations of dye at initial and equilibrium, respectively. V is the volume of the solution (L) and W is the mass of dry sorbent used (g).

The dye removal percentage can be calculated as follows:

$$\text{Removal percentage} = \frac{(C_0 - C_e)}{C_0} \times 100 \quad (3)$$

where C_0 and C_e (mg/L) are the liquid-phase concentrations of dye at initial and equilibrium, respectively.

3. Results and discussion

3.1. Effect of solution pH on dye uptake

Fig. 1 shows the effect of pH on equilibrium adsorption of the MG dye on the RSC at 30 °C. Significant dye adsorption

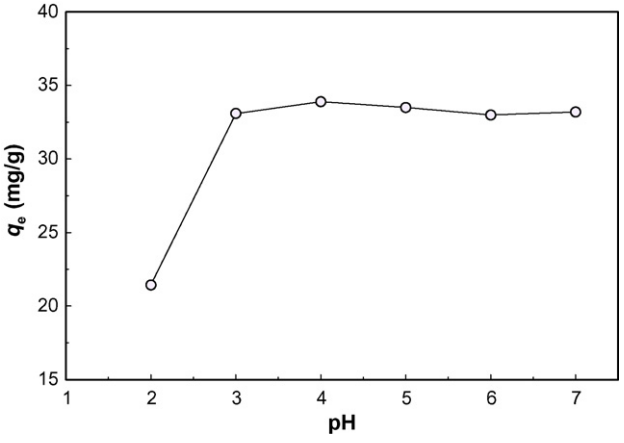

Fig. 1. Effect of initial pH on the adsorption of MG by RSC (initial dye concentration: 50 mg/L; temperature: 30 °C; contact time: 2 h; and RSC dose 1.5 g/L).

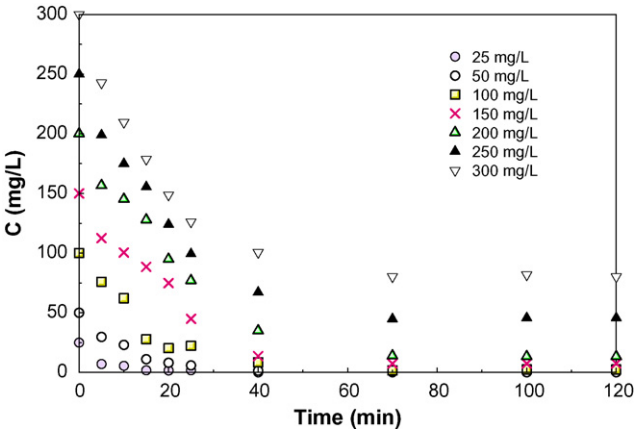

Fig. 2. The adsorption of MG on RSC for different initial concentrations at 30 °C, pH 5, and RSC dose 1.5 g/L.

occurred between pH 3 and 7. At pH less than 3 there was very small amount of removal of dye by the adsorbent. Solution pH would affect both aqueous chemistry and surface binding-sites of the adsorbent. The decrease of sorption at pH less than 3 can be explained by the fact that at this acidic pH, H^+ may compete with dye ions for the adsorption sites of adsorbent, thereby inhibiting the adsorption of dye. Similar result was reported for the adsorption of C.I. basic blue 41 by a natural adsorbent—Silkworm [22].

3.2. Kinetic study

Fig. 2 shows the effect of initial MG concentration, C_0, on the kinetics of adsorption of the dye at pH 5, RSC dosage 0.3 g, and 30 °C. As the initial MG concentration increases from 25 to 300 mg/L the equilibrium removal of MG decreases from 99.9 to 73.3%. It is also noticed in Fig. 2 that large fractions of the total amount adsorbed of MG were removed in the initial rapid uptake phase. In the first 15 min, the fractions of total amounts adsorbed are about 95, 78, 74, 43, 39 and 55% for initial MG concentrations 25, 50, 100, 150, 200 and 300 mg/L, respectively. This is due to the high concentration gradient in the beginning of adsorption which represents a high driving force for the transfer of MG from solution to the surface adsorbent. The results also indicated that the contact time needed for MG solutions with initial concentrations of 25 mg/L to reach equilibrium was 40 min. For MG solutions with initial concentrations of 50-300 mg/L, more than 50 min contact time was required.

The transient behavior of the system at different initial MG concentrations was analyzed using the Lagergren's pseudo-first-order [23] and Ho's pseudo-second-order models [24]. The Lagergren equation models the kinetics of adsorption process as follows:

$$\frac{dq}{dt} = k_1(q_e - q) \tag{4}$$

where q_e is the amount of adsorbate adsorbed at equilibrium (mg/g), q is the amount of adsorbate adsorbed at time t (mg/g) and k_1 is the rate constant of pseudo-first-order adsorption (min^{-1}). Since $q = 0$ at $t = 0$, the initial rate of adsorption can be calculated from Eq. (4) as follows:

$$h_{o,1} = k_1 q_e \tag{5}$$

The integration of Eq. (4) for the boundary conditions $t = 0$–t and $q = 0$–q, gives:

$$q = q_e(1 - e^{-k_1 t}) \tag{6}$$

On the other hand, the pseudo-second-order kinetic equation of Ho is expressed in the form:

$$\frac{dq}{dt} = k_2(q_e - q)^2 \tag{7}$$

where k_2 is the rate constant of pseudo-second-order adsorption (g/mg min) and q_e is the amount of solute adsorbed at equilibrium (mg/g). Integrating Eq. (7) for boundary conditions $t = 0$–t and $q = 0$–q gives:

$$q = \frac{q_e^2 k_2 t}{1 + q_e k_2 t} \tag{8}$$

and the initial rate of adsorption $h_{o,2}$ is:

$$h_{o,2} = k_2 q_e^2 \tag{9}$$

The experimental results of the dye uptake, q, versus time were fitted to both models by the method of non-linear regression. The regression results are shown in Table 1 and Figs. 3 and 4. It can be seen from the plots of q versus t that an increase in initial MG concentration leads to an increase in the adsorption capacity, q_e. As the initial MG concentration increases from 25 to 300 mg/L, the experimentally observed adsorption capacity,

Table 1
Pseudo-first-order and pseudo-second-order rate constants at 30 °C and different initial MG concentrations

C_0	Lagergren's pseudo-first-order model					Pseudo-second-order model			
	q_{exp}	q_e	k_1	$h_{o,1}$	R^2	q_e	k_2	$h_{o,2}$	R^2
25	16.65	16.21	0.2260	3.663	0.9796	17.18	0.02505	7.394	0.9929
50	33.23	33.11	0.09220	3.053	0.9935	36.79	0.003532	4.781	0.9812
100	65.00	65.73	0.06781	4.457	0.9750	75.79	0.001074	6.169	0.9538
150	95.05	98.40	0.04391	4.321	0.9761	119.84	0.0003791	5.443	0.9607
200	124.48	129.17	0.03906	5.045	0.9870	161.11	0.0002368	6.146	0.9745
250	136.24	139.30	0.04711	6.562	0.9936	167.57	0.0003088	8.671	0.9821
300	146.54	147.78	0.05640	8.335	0.9977	173.25	0.0003742	11.232	0.9855

C_0: mg/L; q_e: mg/g; h_o: mg/g min; k_1: min^{-1}; k_2: g/mg min.

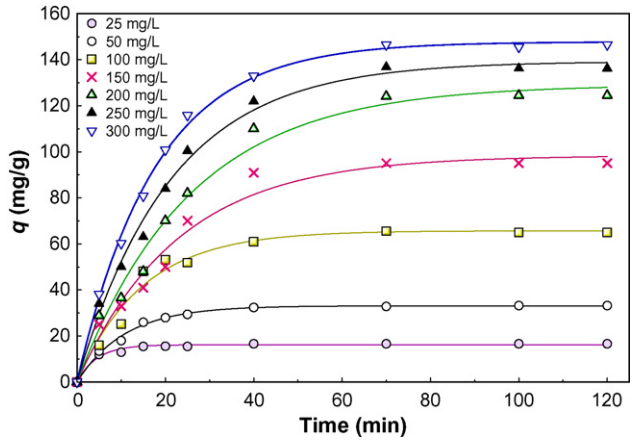

Fig. 3. The fitting of Lagergren's model for MG on RSC for different initial concentrations at 30 °C, pH 5, and RSC dose 1.5 g/L.

q_{exp}, increases from 16.6 to 146.5 mg/g. It is observed from Fig. 3 that for all initial MG concentrations, the adsorption data were well represented by Lagergren's model of Eq. (6) for the entire period of adsorption. The values of adsorption capacity, q_e, calculated from Lagergren's model are close to the values observed experimentally, q_{exp}, with the difference increasing with the increase of initial MG concentration. By examining the values of the coefficient of determination, R^2, it is noticed that the values of R^2 are in the range 0.9750–0.9977. The relatively low R^2 value, 0.9750 and 0.9761 calculated for initial MG concentration 100 and 200 mg/L is due to the scatter of q values in the range 20–40 min. The variance in this time range lowered the value of R^2 and reduced the goodness of fit in the initial period of adsorption; however, the fitted pseudo-first-order curve fitted well in the later stage of adsorption and predicted q_e accurately.

The kinetic data was also analyzed using the pseudo-second-order model of Eq. (8). By comparing Figs. 3 and 4, it is obvious that Lagergren's model fits the experimental data better than the pseudo-second-order model for the entire adsorption period. Also, from the regression results in Table 1, the values of q_e obtained from Lagergeren's model are much closer to the experimental results than q_e obtained from the pseudo-second-order model. By comparing the coefficient of determination, R^2, in Table 1, it is observed that unless for the case of initial MG concentration of 25 mg/L, the pseudo-second-order model fits the experimental results with lower R^2 values (0.9538–0.9855) than Lagergren's model (R^2 from 0.9750–0.9977). The higher R^2 values indicate that the adsorption kinetics data are well represented by Lagergeren's model.

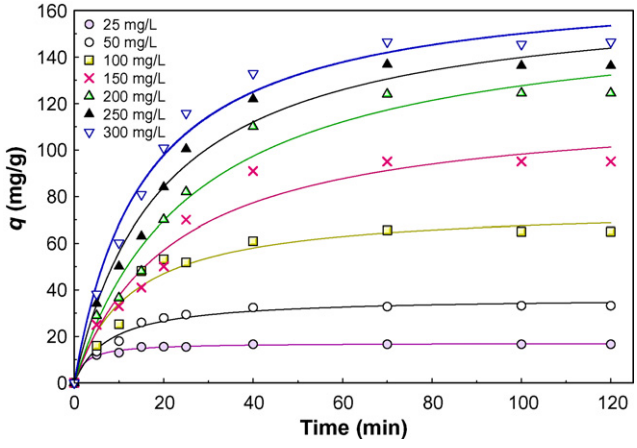

Fig. 4. The fitting of pseudo-second-order model for MG on RSC for different initial concentrations at 30 °C, pH 5, and RSC dose 1.5 g/L.

It is also observed in Table 1 that when the MG initial concentration varies from 25 to 200 mg/L, the rate constant, k_1, decreases from 0.2260 to 0.03906 (mg/g min), but further increase in initial concentration to 300 mg/L causes k_1 to reverse the trend and increase to 0.05640. The non-linear relationships between initial MG concentration and the rate constants suggest that several mechanisms play roles in the adsorption process, such as ion exchange, chelation, and physical adsorption. The values of the initial sorption rate, $h_{o,1}$, are also shown in Table 1. When the initial MG concentration varies from 25 to 300 mg/L, values of $h_{o,1}$ increase from 3.663 to 8.335 (mg/g min). Higher initial rates of adsorption have significant practical importance, because it would facilitate smaller reactor volume ensuring efficiency and economy.

As it was determined that Lagergeren's model is better in predicting the adsorption kinetics at 30 °C and different values of C_0, the values of $q_{e,1}$ (at equilibrium) and q (at any time) were correlated with the initial MG concentration to obtain expressions for these values in terms of C_0 and t as follows:

$$q_{e,1} = 0.8057C_0 - 0.0010074C_0^2 \quad (R^2 = 0.9943) \tag{10}$$

$$q = 8.729 + 1.958 \times 10^{-2}C_0t - 2.3788 \times 10^{-4}C_0t^2 + 9.2022 \times 10^{-7}C_0t^3 \quad (R^2 = 0.9733) \tag{11}$$

Eq. (11) can be used to predict the amount of MG adsorbed for any given C_0 and contact time, pH 5, and RSC dose 0.3 g. The

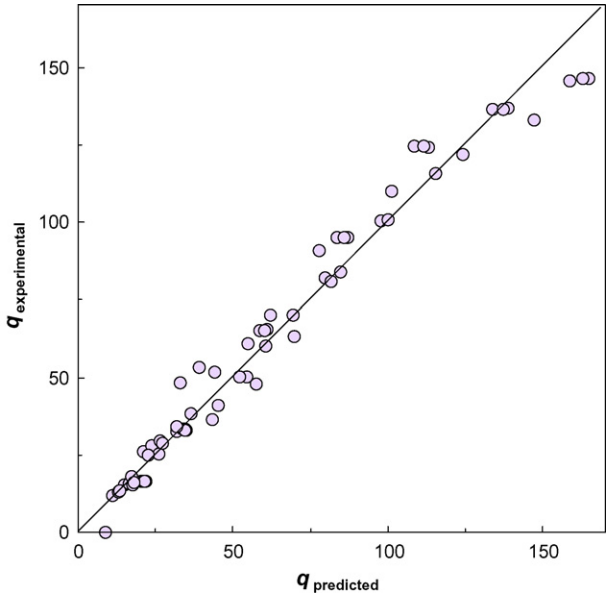

Fig. 5. Plot of experimentally determined q_e versus values of q_e predicted from Eq. (8).

predicted and experimental values of q at different times and initial MG concentrations are plotted in Fig. 5.

3.3. Sorption mechanism

The kinetic studies help in identifying and predicting the adsorption process, but the determination of the sorption mechanism is also important for design purposes. In a solid–liquid adsorption process, the transfer of the adsorbate is characterized by either boundary-layer diffusion (external mass transfer) or intraparticle diffusion (mass transfer through the pores), or by both. It is generally accepted that the adsorption dynamics consists of three consecutive steps [25]:

- Transport of adsorbate molecules from the bulk solution to the adsorbent external surface by diffusion through the boundary layer.
- Diffusion of the adsorbate from the external surface into the pores of the adsorbent.
- Adsorption of the adsorbate on the active sites on the internal surface of the pores.

The last step, adsorption, is usually very rapid in comparison to the first two steps. Therefore, the overall rate of adsorption is controlled by either film or intraparticle diffusion, or a combination of both. Many studies have shown that the boundary-layer diffusion is the rate controlling step in systems characterized by dilute concentrations of adsorbate, poor mixing, and small particle size of adsorbent. Whereas the intraparticle diffusion controls the rate of adsorption in systems characterized by high concentrations of adsorbate, good mixing, and big particle size of adsorbent [26,27]. Also, it has been noticed in many systems that boundary-layer diffusion (external mass transfer) is dominant at the beginning of adsorption during the initial adsorbate uptake, then gradually the adsorption rate becomes controlled by intraparticle diffusion after the adsorbent's external surface is loaded with the adsorbate [25–27].

The intraparticle diffusion parameter, k_i (mg/g min$^{0.5}$) is defined by equation [28]:

$$q = k_i t^{0.5} + c \quad (12)$$

where q is the amount of MG adsorbed (mg/g) at time t, k_i is intraparticle diffusion constant (mg/g min$^{0.5}$), and c is an arbitrary constant the represents the thickness (or resistance) of the boundary layer.

Theoretically, the plot of k_i versus $t^{0.5}$ should show at least four linear regions that represent boundary-layer diffusion, followed by intraparticle diffusion in macro, meso, and micro pores [29]. These four regions are followed by a horizontal line representing the system at equilibrium. The intraparticle diffusion plots of the experimental results, q versus $t^{0.5}$ for different initial MG concentrations at 30 °C and RSC dose of 0.30 g are shown in Fig. 6. From the figure it is observed that there are three linear regions. At the beginning of adsorption there is a linear region representing the rapid surface loading, followed a linear region representing pore diffusion, and finally a horizontal linear region representing equilibrium. The method of piecewise linear regression was used to avoid subjective judgment in choosing the beginning and end of each region. The results of piecewise linear regression are shown in Table 2 and the lines representing intraparticle diffusion are plotted in Fig. 6. It is observed that the time elapsed until pore diffusion starts controlling the rate of adsorption increases from 11 to 25 min when the initial MG concentration increases from 25 to 100 mg/L, but on further increase of initial MG concentration above 100 mg/L the elapsed time to the start of diffusion control drops gradually to 9 min. The intraparticle diffusion parameter, k_i, is determined from the slope of the second linear region while the intercept is proportional to the boundary-layer thickness (or resistance). The calculated values of k_i and the intercept are shown in Table 2. It is obvious that values of k_i increase rapidly from 0.484 to 20.92 when the initial MG concentration is increased from 25 to 150 mg/L. Further increase in the initial MG concentration from 150 to 300 mg/L has little effect on k_i. It is also observed that the value of the intercept increases from 13.43 to 34.31 when C_0 is increased from 25 to 100 mg/L, which indicates that the thickness (or the resistance to mass transfer) of the boundary layer increases significantly with increase of C_0 in this range. However, on further increase of C_0 above 100 mg/L the values of the slope decrease indicating a decrease in the resistance to mass transfer in the external boundary layer. It is interesting to note that the value of the intercept drops sharply when C_0 is 150 mg/L, coinciding with the above mentioned drop in the time elapsed during film-

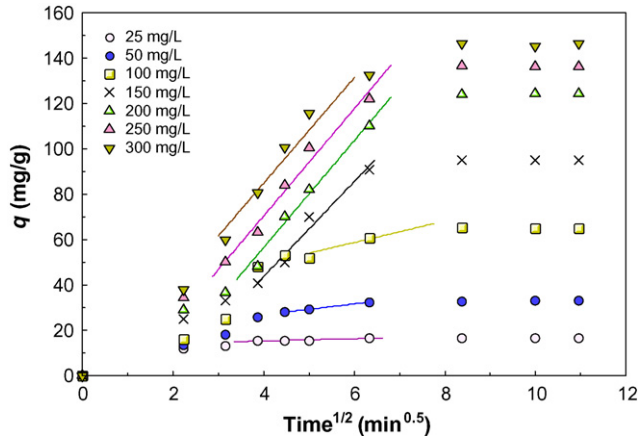

Fig. 6. Intraparticle diffusion plot for the adsorption at 30 °C and different initial MG concentrations (pH: 5; RSC dose: 1.5 g/L).

Table 2
Diffusion coefficients for adsorption of MG on RSC at 30 °C, pH 5, and different initial concentrations

C_0	C	k_i	k_s	$D_i \times 10^6$
25	13.43	0.484	0.1180	8.37
50	17.50	2.362	0.0745	4.22
100	34.31	3.940	0.0486	3.80
150	−39.83	20.92	0.0414	1.58
200	−42.86	24.49	0.0224	1.72
250	−24.27	23.69	0.0337	1.86
300	−8.28	23.31	0.0352	2.43

C_0: mg/L; c: mg/g; k_i: mg/g min$^{0.5}$; k_s: min^{-1}; D_i: cm^2/s.

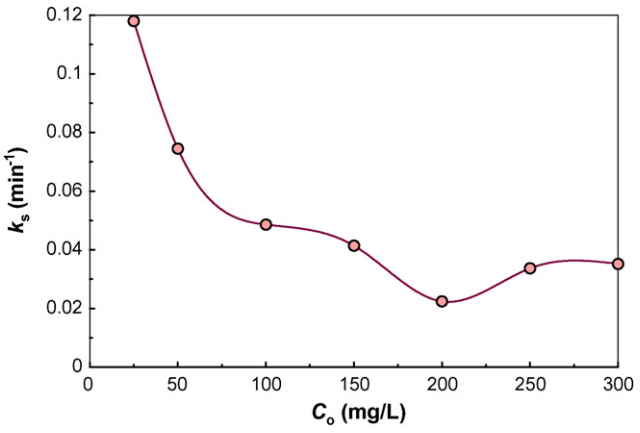

Fig. 7. Plots of the rate constant of external mass transfer, k_s, versus C_0 for the initial stage of adsorption at 30 °C and different initial MG concentrations (pH: 5; RSC dose: 1.5 g/L).

diffusion control, and also for C_0 of 150 mg/L and higher, the slope of the first linear region (film-diffusion control) becomes less than the slope of the second linear region (pore diffusion control).

The rate constants of external mass transfer were calculated using the plot of C/C_0 against time at different initial MG concentrations (figure not shown). The experimental results were fitted to second order polynomial, then the slopes were calculated from the first derivative of the polynomial functions. The values of initial adsorption rates, k_s (min^{-1}) are plotted in Fig. 7. It is observed that the rate in the initial period of adsorption, where external mass transfer is assumed to predominate, decreases sharply with increase of C_0, which can be expected due to the increase in boundary-layer resistance exhibited in the values of the intercept in intraparticle diffusion plots, then at higher initial MG concentrations (above 200 mg/L) the values of k_s increases slightly.

The decrease of k_s with increasing C_0 is not in agreement with the trend of $h_{o,1}$ predicted from Lagergren's model but agrees with the trend of $h_{o,2}$ predicted from the pseudo-second-order model shown in Table 1. The reason for this discrepancy may be that the fitting of the pseudo kinetic models was performed on the experimental results of the entire time period of adsorption, thus affecting the estimates for the initial stage.

In order to corroborate the actual rate controlling steps in MG adsorption on RSC, the experimental data was further analyzed by the expression of Boyd et al. [30]:

$$F = 1 - \frac{6}{\pi^2}\exp(-Bt) \tag{13}$$

where F is the fractional attainment of equilibrium, at different times, t, and Bt is a function of F

$$F = \frac{q_t}{q_e} \tag{14}$$

where q_t and q_e are the dye uptake (mg/g) at time t and at equilibrium, respectively.

Eq. (13) can be rearranged to

$$Bt = -0.4977 - \ln(1 - F) \tag{15}$$

The values of Bt were calculated from Eq. (15) and plotted against time as shown in Fig. 8. The plots are linear only in the initial period of adsorption and do not pass through the origin, indicating that external mass transfer is the rate limiting process in the beginning of adsorption. The calculated values of B were used to determine the effective diffusion coefficient, D_i (cm^2/s) from the equation:

$$B = \frac{\pi^2 D_i}{r^2} \tag{16}$$

where r is the radius of the adsorbent particle assuming spherical shape. The values of D_i in Table 2 show that the relation between C_0 and the effective diffusion coefficient, D_i, has the same general trend as k_s and this trend may be related to the increasing dimerization of MG with the increase of its concentration [31,32]. Also, by examining Fig. 8, it can be seen that the initial period where external mass transfer is the rate controlling step decreases from 25 to 10 min when C_0 increases from 25 to 300 mg/L.

3.4. Equilibrium modeling

Although there are many adsorption isotherms in the literature, the most widely used by researchers are two of the oldest isotherms, namely Freundlich [33] and Langmuir [34] isotherms.

The Freundlich isotherm is the first known relationship describing the adsorption equation. This isotherm can be used for non-ideal adsorption on heterogeneous surfaces. The heterogeneity arises from the presence of different functional groups on the surface, and the various adsorbent–adsorbate interactions. The Freundlich isotherm is expressed by the following empirical equation:

$$q_e = K_F C_e^{1/n} \tag{17}$$

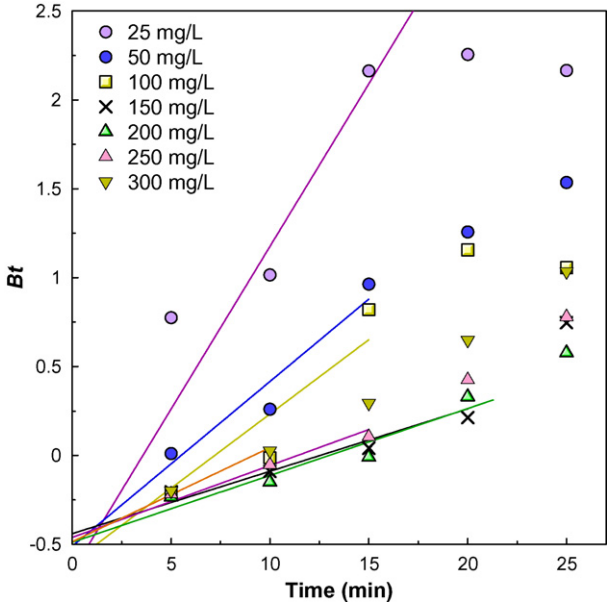

Fig. 8. Boyd plots for MG adsorption at 30 °C and different initial MG concentrations (pH: 5; RSC dose: 1.5 g/L).

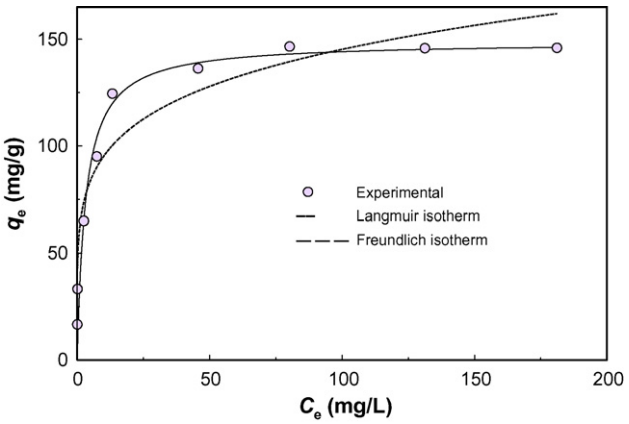

Fig. 9. The fitting of Freundlich and Langmuir isotherm models to adsorption equilibrium results of MG on RSC at 30 °C, pH 5, and RSC dose 1.5 g/L.

where K_F is the Freundlich adsorption constant ((mg/g)(L/g)^n) and $1/n$ is a measure of the adsorption intensity.

The development of the Langmuir isotherm assumes monolayer adsorption on a homogenous surface. It is expressed by the following equation:

$$q_e = \frac{q_m K_a C_e}{1 + K_a C_e} \quad (18)$$

where C_e is the equilibrium concentration (mg/L), q_e the amount adsorbed (mg/g), q_m is q_e for complete monolayer adsorption capacity (mg/g), and K_a is the equilibrium adsorption constant (L/mg).

The experimental equilibrium results were fitted by non-linear regression to the Freundlich and Langmuir isotherm models. Fig. 9 and Table 3 show that the Langmuir isotherm gave a better fitting to the experimental results ($R^2 = 0.9487$) than the Freundlich isotherm ($R^2 = 0.9295$) which suggests that adsorption takes place by monolayer adsorption on a homogeneous surface. Similar result was reported for the adsorption of malachite green on arundo donax root carbon (ADRC) [35].

3.5. Comparison of various adsorbents

Table 4 compares the adsorption capacity of different types of adsorbents used for removal of malachite green. The most important parameter to compare is the Langmuir q_m value since it is a measure of adsorption capacity of the adsorbent. The value of q_m in this study is larger than those in most of previous works. This suggests that MG could be easily adsorbed on RSC. The results indicated that the RSC can be considered a promising adsorbent for the removal of MG from aqueous solutions.

Table 3
Isotherm constants for MG adsorption on RSC at 30 °C and pH 5

Langmuir isotherm			Freundlich isotherm		
q_m (mg/g)	K_a (L/mg)	R^2	K_f ((mg/g)(L/g)^n)	$1/n$	R^2
148.74	0.313	0.9487	62.36	0.184	0.9295

Table 4
Comparison of adsorption capacities of various adsorbents for malachite green

Adsorbent	q_m (mg/g)	T (°C)	Reference
Rice straw char (RSC)	148.74	30	This work
Arundo donax root carbon (ADRC)	8.70	30	[35]
Activated charcoal	0.179	30	[36]
Bentonite clay	7.72	35	[37]
Waste apricot	116.27	30	[38]
Activated carbon	149	25	[39]
Bagasse fly ash (BFA)	170.33	30 ± 1	[40]
Activated carbons commercial grade (ACC)	8.27	30 ± 1	[40]
Laboratory grade activated carbons (ACL)	42.18	30 ± 1	[40]

4. Conclusions

(1) The present study shows that the char rice husk, an abundant agricultural waste, can be used as an adsorbent for the removal of malachite green dye from aqueous solutions.
(2) The amount of dye adsorbed was found to vary with initial malachite green concentration and contact time.
(3) The adsorption equilibrium data were found to fit the Langmuir isotherm, indicating monolayer adsorption on a homogenous surface.
(4) Lagergren's pseudo-first-order model can be used to predict the adsorption kinetics.
(5) The overall rate of dye uptake was found to be controlled by external mass transfer at the beginning of adsorption, while intraparticle diffusion controlled the overall rate of adsorption at a later stage.

References

[1] S. Srivastava, R. Sinha, D. Roy, Toxicological effects of malachite green, Aquat. Toxicol. 66 (2004) 319–329.
[2] C.F. Chang, C.H. Yang, Y.O. Shu, T.I. Chen, M.S. Shu, I.C. Liao, Effects of temperature, salinity and chemical drugs on the in vitro propagation of the Dinoflagellate parasite, *Amylodinium cellatum*, Asian Fish Soc. (2001) P31.
[3] R.A. Schnick, The impetus to register new therapeutants for aquaculture, Prog. Fish Cult. 50 (1988) 190–196.
[4] I.A. Rahman, B. Saad, S. Shaidan, E.S. Sya Rizal, Adsorption characteristics of malachite green on activated carbon derived from rice husks produced by chemical–thermal process, Bioresour. Technol. 96 (2005) 1578–1583.
[5] J.C. Sandra, R.B. Lonnie, F.K. Donna, R.D. Daniel, T. Louis, A.B. Frederick, Toxicity and metabolism of malachite green and leucomalachite green during short-term feeding to Fischer 344 rats and B6C3F1 mice, Chem-Biol. Interact. 122 (1999) 153–170.
[6] R.F.P. Nogueira, M.R.A. Silva, A.G. Trovó, Influence of the iron source on the solar photo-Fenton degradation of different classes of organic compounds, Solar Energy 79 (2005) 384–392.
[7] K. Wu, Y. Xie, J. Zhao, H. Hidaka, Photo-Fenton degradation of a dye under visible light Irradiation, J. Mol. Catal. A: Chem. 144 (1999) 77–84.
[8] C. Hachem, F. Bocquillon, O. Zahraa, M. Bouchy, Decolourization of textile industry wastewater by the photocatalytic degradation process, Dyes Pigments 49 (2001) 117–125.
[9] H. Kominami, H. Kumamoto, Y. Kera, B. Ohtani, Photocatalytic decolorization and mineralization of malachite green in an aqueous suspension of titanium(IV) oxide nano-particles under aerated conditions: correla-

tion between some physical properties and their photocatalytic activity, J. Photochem. Photobiol. A: Chem. 160 (2003) 99–104.
[10] F. Sayılkan, M. Asiltürk, P. Tatar, N. Kiraz, E. Arpaç, H. Sayılkan, Photocatalytic performance of Sn-doped TiO_2 nanostructured mono and double layer thin films for Malachite Green dye degradation under UV and vis-lights, J. Hazard. Mater. 144 (2007) 140–146.
[11] S. Rajgopal, T. Karthikeyan, B.G. Prakash Kumar, L.R. Miranda, Utilization of fluidized bed reactor for the production of adsorbents in removal of malachite green, Chem. Eng. J. 116 (2006) 211–217.
[12] A. Mittal, L. Krishnan, V.K. Gupta, Removal and recovery of malachite green from wastewater using an agricultural waste material, de-oiled soya, Sep. Purif. Technol. 43 (2005) 125–133.
[13] V.K. Garg, R. Kumar, R. Gupta, Removal of malachite green dye from aqueous solution by adsorption using agro-industry waste: a case study of *Prosopis cineraria*, Dyes Pigments 62 (2004) 1–10.
[14] V.K. Gupta, A. Mittal, L. Krishnan, V. Gajbe, Adsorption kinetics and column operations for the removal and recovery of malachite green from wastewater using bottom ash, Sep. Purif. Technol. 40 (2004) 87–96.
[15] A. Mittal, Adsorption kinetics of removal of a toxic dye, Malachite Green, from wastewater by using hen feathers, J. Hazard. Mater. B133 (2006) 196–202.
[16] P. Janoš, V. Šmídová, Effects of surfactants on the adsorptive removal of basic dyes from water using an organomineral sorbent-iron humate, J. Colloid Interface Sci. 291 (2005) 19–27.
[17] R. Gong, Y. Jin, F. Chen, J. Chen, Z. Liu, Enhanced malachite green removal from aqueous solution by citric acid modified rice straw, J. Hazard. Mater. 137 (2006) 865–870.
[18] P.J. Van Soest, Rice straw, the role of silica and treatments to improve quality, Anim. Feed Sci. Technol. 130 (2006) 137–171.
[19] D.I. Hills, D.W. Roberts, Anaerobic digestion of dairy manure and field crop residues, Agric. Waste 3 (1981) 179–189.
[20] B.L. Maiorella, Ethanol, in: M. Young (Ed.), Comprehensive Biotechnology, vol. 3, Pergamon Press, Oxford, 1985, pp. 861–914.
[21] K. Karimi, S. Kheradmandinia, M.J. Taherzadeh, Conversion of rice straw to sugars by dilute-acid hydrolysis, Biomass Bioenergy 30 (2006) 247–253.
[22] B. Noroozi, G.A. Sorial, H. Bahrami, M. Arami, Equilibrium and kinetic adsorption study of a cationic dye by a natural adsorbent—Silkworm pupa, J. Hazard. Mater. B139 (2007) 167–174.
[23] S. Lagergren, Zur theorie der sogenannten adsorption geloster stoffe. Kungliga Svenska Vetenskapsakademiens, Handlingar 24 (4) (1898) 1–39.
[24] Y.S. Ho, Adsorption of heavy metals from waste streams by peat, Ph.D. Thesis, University of Birmingham, Birmingham, U.K., 1995.
[25] B. Koumanova, P. Peeva, S. Allen, Variation of intraparticle diffusion parameter during adsorption of *p*-chlorophenol onto activated carbon made from apricot stones, J. Chem. Technol. Biotechnol. 78 (2003) 582–587.
[26] D. Mohan, K.P. Singh, Single and multicomponent adsorption of cadmium and zinc using activated carbon derived from bagasse—an agricultural waste, Water Res. 36 (2004) 2304–2318.
[27] M.S. Ray, Adsorption and adsorptive separations: a review and bibliographical update, Adsorption 2 (1996) 157–178.
[28] W.J. Weber Jr., J.C. Morris, Kinetics of adsorption on carbon from solution, J. Sanit. Eng. Div. Proc. Am. Soc. Civil Eng. 89 (1963) 31–59.
[29] Y.S. Ho, G. McKay, The kinetics of sorption of basic dyes from aqueous solution by Sphagnum moss peat, Can. J. Chem. Eng. 76 (1998) 822–827.
[30] G.E. Boyd, A.W. Adamson, L.S. Myers Jr., The exchange adsorption of ions from aqueous solutions by organic zeolites. II: Kinetics, J. Am. Chem. Soc. 69 (1947) 2836–2848.
[31] N. Strataki, V. Bekiari, P. Lianos, Study of the conditions affecting dye adsorption on titania films and of their effect on dye photodegradation rates, J. Hazard. Mater. 146 (2007) 514–519.
[32] R.N. Muir, A.J. Alexander, Structure of monolayer dye films studied by Brewster angle cavity ringdown spectroscopy, Phys. Chem. Chem. Phys. 5 (2003) 1279–1283.
[33] H.M.F. Freundlich, Uber Die Adsorption in Losungen, Zeitschrift fur Physikalische Chemie 57 (1906) 385.
[34] I. Langmuir, Constitution and fundamental properties of solids and liquids. I: Solids, J. Am. Chem. Soc. 38 (1916) 2221.
[35] J. Zhang, et al., Adsorption of malachite green from aqueous solution onto carbon prepared from Arundo donax root, J. Hazard. Mater. 150 (2008) 774–782.
[36] M.J. Iqbal, M.N. Ashiq, Adsorption of dyes from aqueous solutions on activated charcoal, J. Hazard. Mater. B139 (2007) 57–66.
[37] S.S. Tahir, N. Rauf, Removal of a cationic dye from aqueous solutions by adsorption onto bentonite clay, Chemosphere 63 (2006) 1842–1848.
[38] C.A. Başar, Applicability of the various adsorption models of three dyes adsorption onto activated carbon prepared apricot, J. Hazard. Mater. B135 (2006) 232–241.
[39] Y. Önal, C. Akmil-Başar, C. Sarıcı-Ö zdemir, Investigation kinetics mechanisms of adsorption malachite green onto activated carbon, J. Hazard. Mater. 146 (2007) 194–203.
[40] I.D. Mall, V.C. Srivastava, N.K. Agarwal, I.M. Mishra, Adsorptive removal of malachite green dye from aqueous solution by bagasse fly ash and activated carbon-kinetic study and equilibrium isotherm analyses, Colloids Surf. A: Physicochem. Eng. Asp. 264 (2005) 17–28.